ENGINEERING

Wearable thermoelectrics for personalized thermoregulation

Sahngki Hong[1,2], Yue Gu[1,3], Joon Kyo Seo[1,3], Joseph Wang[1,3], Ping Liu[1,3], Y. Shirley Meng[1,3,4], Sheng Xu[1,3]*, Renkun Chen[1,2,4]*

Thermoregulation has substantial implications for energy consumption and human comfort and health. However, cooling technology has remained largely unchanged for more than a century and still relies on cooling the entire space regardless of the number of occupants. Personalized thermoregulation by thermoelectric devices (TEDs) can markedly reduce the cooling volume and meet individual cooling needs but has yet to be realized because of the lack of flexible TEDs with sustainable high cooling performance. Here, we demonstrate a wearable TED that can deliver more than 10°C cooling effect with a high coefficient of performance (COP > 1.5). Our TED is the first to achieve long-term active cooling with high flexibility, due to a novel design of double elastomer layers and high-ZT rigid TE pillars. Thermoregulation based on these devices may enable a shift from centralized cooling toward personalized cooling with the benefits of substantially lower energy consumption and improved human comfort.

INTRODUCTION

Thermoregulation not only plays a vital role in human comfort and health but also contributes significantly to energy consumption. The heating and cooling of buildings alone currently accounts for more than 10% of the total energy consumed globally (*1*); this high level of energy consumption and the accompanying environmental impact, i.e., the emission of potent global warming gases, are expected to increase markedly with the rapid growth of economies (*2*). Climate control systems are also used to achieve thermal comfort in electric vehicles; however, these systems can drain up to 40% of battery power in adverse weather conditions, presenting a major roadblock to achieving long driving ranges (*3*).

The ongoing effort to reduce the energy consumption of climate control systems has mainly focused on the development of more efficient thermoregulation technologies (*4*). However, a substantial amount of energy is wasted by traditional climate control systems, as they heat/cool entire buildings or vehicles, although the occupants only occupy a small space. The large amount of wasted energy is evident when considering the great disparity between human metabolic rate (100 to 150 W) (*5*) and per capita heating, ventilation, and air conditioning (HVAC) energy consumption rate in the United States (~1.5 kW) (*1*). Moreover, it is difficult to set the temperature of an entire building or vehicle to ensure the thermal comfort of all the occupants or passengers as thermal comfort conditions can vary significantly from person to person (*6*). In addition to the implications for energy efficiency of buildings and vehicular thermal envelops, there is also tremendous interest in achieving optimal thermal comfort for various outdoor application scenarios, such as those encountered in sports, military, special occupations, and health care (*7*).

Recently, there has been growing interest in personal thermoregulation devices (*8*, *9*), which can deliver a precise thermal dose to target spots on individuals and consequently reduce the heating or cooling volume by orders of magnitude compared with building/vehicular-level thermal envelops. While the traditional heating/cooling system has an advantage in covering large space with high cooling/heating capacity and efficiency, which is suitable for applications in large-scale buildings with a large number of occupants, or when the ambient temperature is significantly deviated from the thermal comfort temperature, it is also desirable to use personalized thermoregulation in both indoor and outdoor scenarios for energy efficiency purposes when the number of occupants to be cooled/heated is small or for enhanced comfort and health for individuals with different thermal comfort zones. For instance, if building set temperature can be increased by 7°C with assistance of the devices in hot climates, then it is expected to save ~70% of energy consumed by a centralized system (*10*). The personal thermoregulation devices are also useful for outdoor heating or cooling, where centralized heating or AC is not available. In particular, the personal cooling devices could find applications to improve the health of outdoor athletes and people of special occupations (e.g., fire fighters and construction workers), who could be exposed to intense heat, against heat stroke or burn. These devices could also be potentially used to manage multiple symptoms and conditions, such as sclerosis, fever, burn wound, and neurologic disorders (*7*). Application of personal thermoregulation devices in the military also has large potential; the devices would not only be able to provide thermal protection but could also be capable of hiding thermal infrared (IR) signature from human body for thermal camouflage against IR detection.

Heating garments that exploit Joule heating, such as metallic nanowire meshes (*9*), are an example of these personal thermoregulation devices. However, the development of active cooling garments is far more challenging and largely unexplored as most current cooling devices are bulky and difficult to integrate into a garment. For instance, commercially available cooling vests contain bulky fluidic channels for coolant circulation or water/ice packs, and their cooling power is not adjustable (*7*). Given these inherent drawbacks of fluidic-based personal cooling garments, current studies are focused primarily on solid-state technologies such as electrocaloric (*11*), magnetocaloric (*12*), and thermoelectric (TE) cooling systems (*13*). Nevertheless, despite extensive material-level studies, wearable devices with high cooling performance have yet to be demonstrated. Active cooling was recently demonstrated in miniaturized electrocaloric devices (*14*) with a high voltage (~10 kV); however, the temperature drop remained small (1.4°C).

[1]Materials Science and Engineering Program, University of California, San Diego, La Jolla, CA 92093, USA. [2]Department of Mechanical and Aerospace Engineering, University of California, San Diego, La Jolla, CA 92093, USA. [3]Department of NanoEngineering, University of California, San Diego, La Jolla, CA 92093, USA. [4]Sustainable Power and Energy Center, University of California, San Diego, La Jolla, CA 92093, USA.
*Corresponding author. Email: shengxu@eng.ucsd.edu (S.X.); rkchen@ucsd.edu (R.C.)

Thermoelectric devices (TEDs) are especially attractive for personalized cooling application, as they are solid state with small form factors and the cooling power is readily adjustable. Although there has been substantial work on flexible TEDs for wearable applications (*15*–*35*), most of these devices have only achieved power generation by harnessing body heat (*17*–*35*) or have shown limited cooling effect with the assistance of bulky heat sinks (such as water gels or fans) (*29*, *30*). To the best of our knowledge, none of these wearable TEDs have shown long-term (e.g., >1 hour) active cooling without the use of bulky heat sinks. Although various wearable TE power generators can, in principle, be used for cooling, the requirement of achieving active cooling, that is, pumping the heat from the cold to hot side, is substantially more stringent. A wearable TED capable of power generation is not necessarily suitable for active cooling: The Peltier cooling power on the cold side must overcome the parasitic heating effects of both the heat conduction from the hot side and Joule heating; in addition, the heat pumped to the hot side must be efficiently dissipated into the environment (hence, the need for bulky heat sinks). Fundamentally, the devices must have high performance (measured by the TE figure of merit, ZT) with a suitable thermal design. Some previously reported TEDs have only shown power generation capability (*17*–*28*, *31*–*35*); however, none have exhibited sustainable active cooling performance without the aid of a water heat sink (*29*, *30*), primarily because of the low performance of flexible TE materials [e.g., polymers or organic/inorganic hybrids (*36*) with ZT < 0.42] or unoptimized thermal design for cooling even with high-performance Bi-Te–based TE materials (*17*–*26*).

Here, we designed and demonstrated the first flexible and wearable TED with long-term (>8 hours) and large (>10°C) active cooling effect by addressing the aforementioned challenges. Our TED design uses an innovative fabrication scheme of sandwiching rigid inorganic high-ZT TE pillars between stretchable elastomer sheets and, by virtue of the novel thermal design, demonstrates a large cooling effect of more than 10°C to the skin without the use of any heat sinks. Although active cooling data are not available for previously reported wearable TEDs, our flexible TED exhibits significantly higher power output when used as a power generator from body heat than previous TEDs [up to 4.5 to 25.1 μW cm^{-2} in our TED versus 10^{-3} to 2.28 μW cm^{-2} in previous TEDs (*18*–*26*)]. We also integrated the TED into a wearable garment with long-term, energy-efficient cooling and heating effects on human skin: The garment kept the skin at the thermal comfort temperature of 32°C, while the ambient temperature varied within the large range of 22° to 36°C. Last, an all-flexible personalized thermoregulation package was demonstrated by integrating a flexible battery pack into the TED garment. Our flexible and high-performance TED design may pave the way for personalized cooling with the benefits of substantial energy savings and improved thermal comfort.

RESULTS AND DISCUSSION

Design, fabrication, and characterization of flexible TED

We used a novel concept of double elastomer layer design embedding an air gap insulation layer between two stretchable sheets and high-ZT inorganic TE pillars with optimized aspect ratio and spatial density. This design simultaneously maximizes the device flexibility and minimizes the thermal leakage through the TED, eventually resulting in high cooling performance. A schematic illustration and photograph of our TED are presented in Fig. 1 (A to C). To achieve mechanical flexibility and high cooling performance, we used the double elastomer layer design, sandwiching rigid TE pillars (1 mm by 1 mm in cross section and 5 mm in height, with a 3-mm gap between pillars) between two 1-mm-thick stretchable Ecoflex sheets separated by a 4-mm air gap (Fig. 1C). The top and bottom 0.5-mm-long segments of the TE pillars were embedded in the Ecoflex sheets. This double-layer design provides sufficient flexibility despite the rigidity and high aspect ratio of the TE pillars and greatly enhances the cooling effect. As shown in Fig. 1D, when the TED with the double-layer design is bent, the top stretchable sheet expands, while the bottom sheet contracts, and our finite element simulation showed that the bending stiffness of the double-layer design is only 30% of the conventional single elastomer layer design (Fig. 1E), which can be found in most of the previous flexible TEDs (*17*–*26*, *28*). The fabrication process of our TED is presented in Fig. 1F and described in detail in Materials and Methods. Photographs of the devices during the intermediate fabrication steps are shown in fig. S1 (A to D). Including all the components, the TED remains thin (6 mm) and light (0.56 g cm^{-2}) [see fig. S1 (E and F)] compared to conventional cooling garments (*7*) or TEDs with bulky heat sinks (*29*, *30*).

The salient features of the thermal design in our TED include the high aspect ratio (height/width, 5:1) of the pillars with low spatial density (6.25%) and the large air gap between the stretchable sheets (4 mm), which result in small thermal conductance between the cold and hot sides of the TED. The conductance of TED (G_{TED}) is calculated on the basis of $G_{TED} = Nk_{TE}A_{TE}/L_{TE}$, where N, k_{TE}, A_{TE}, and L_{TE} are the number, thermal conductivity, cross-sectional area, and length of the TE pillars, respectively. The calculated G_{TED} of our design is ~ 30 W m^{-2} K^{-1}, which is 50% lower than that of the conventional single-layer design (Fig. 1E). This low G_{TED} is comparable to the heat transfer coefficient between the TED and air (h_{air} ~ 10 to 20 W m^{-2} K^{-1}) resulting from natural convection and radiation (*37*). This thermal resistance matching ensures that the heat pumped from the cold (skin) side and the Joule heating will dissipate into the air rather than flow back to the skin (Fig. 1C and derivation in note S1). If G_{TED} were substantially higher, an efficient heat sink would be needed to match h_{air} with G_{TED}, such as that used in previous wearable TEDs (*27*–*30*). However, there is also a limit to the continuous reduction of G_{TED} by applying taller and smaller pillars, as excessively taller and smaller pillars would result in larger electrical resistance and Joule heating and compromise the device flexibility and mechanical strength (fig. S2 and Fig. 1E). In addition, the large distance between adjacent TE pillars requires efficient lateral heat spreading to ensure that a uniform temperature is maintained within each of the Ecoflex layers; this heat spreading was achieved by embedding AlN microparticles into the Ecoflex to increase its lateral thermal conductivity.

The basic TE and mechanical characteristics of the fabricated flexible TED are shown in Fig. 2. As discussed, reducing G_{TED} is imperative to achieve active cooling without resorting to the use of bulky heat sinks. The measured G_{TED} was 32 W m^{-2} K^{-1} (Fig. 2A), which falls within the optimal range for the cooling of human skin at a typical metabolic rate (50 to 100 W m^{-2}) (*5*). The corresponding average thermal conductivity of the TE pillars was determined to be 1.52 W m^{-1} K^{-1}. The average Seebeck coefficient (S) of the TED at the device level was measured to be 196 μV K^{-1} pillar (Fig. 2B). Last, the overall electrical resistance of the TED was measured to be 7.9 ohm, yielding an average electrical conductivity (σ) of 932 S cm^{-1}. The corresponding device-level ZT was determined to be 0.71 at room temperature. This ZT value is consistent with that of the constituent n- and p-type materials with the same compositions previously studied by us (*31*), indicating the minimal influence of our device

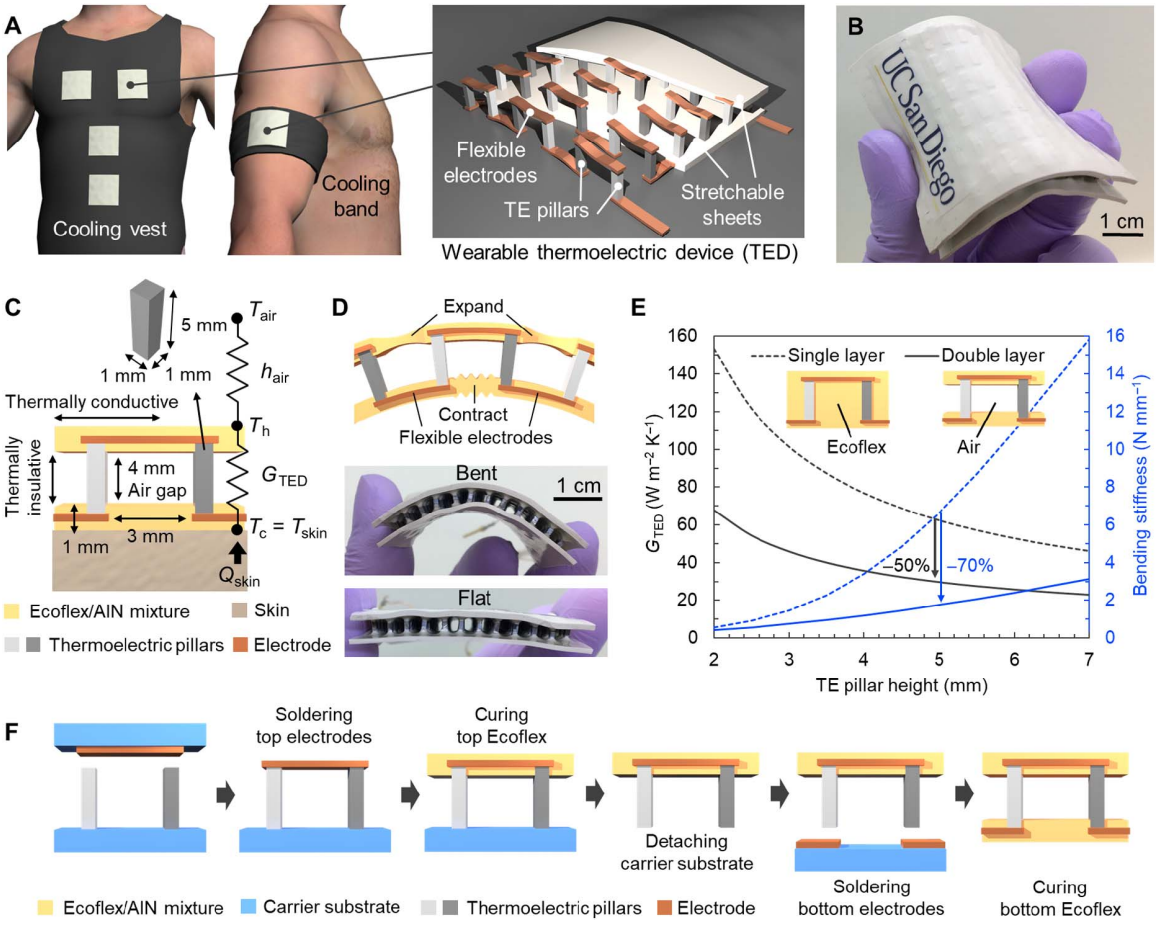

Fig. 1. TED design and fabrication process. (**A**) Schematic illustration of cooling garments with wearable TEDs (left). The internal structure of the wearable TED with TE pillars connected by flexible copper electrodes and sandwiched between two stretchable sheets (right). (**B**) Photograph of the fabricated 5 cm by 5 cm flexible TED. (**C**) Schematic illustration of TED design. The low thermal conduction inside the TED and high thermal conduction within the stretchable sheets are the key features of the design used to achieve the cooling effect. (**D**) Schematic diagram and photographs showing the flexibility of the TED. The double-layer design of stretchable sheets enhances the flexibility. During bending, the top stretchable sheet expands, while the bottom stretchable sheet contracts. (**E**) Finite element simulation comparison of G_{TED} and the bending stiffness of double- and single-layer designs of flexible TEDs as a function of TE pillar height. The double-layer design reduces G_{TED} by 50% and the bending stiffness by 70% compared to those of the single-layer design. (**F**) Fabrication process of the TED (see Materials and Methods for details). Photo credit: Sahngki Hong, University of California, San Diego.

fabrication process on the material properties and high-quality interfaces for thermal and electrical transport.

The lateral thermal conductivity of the stretchable sheet (k_p) with embedded AlN particles (26 volume %) was measured to be 0.77 W m^{-1} K^{-1}, which represents an approximately fourfold enhancement over that of pristine Ecoflex (0.20 W m^{-1} K^{-1}), as shown in Fig. 2C. Incorporating all of these material properties, our finite element simulation indicated that the flexible TED is expected to provide ~7°C of maximum cooling with only natural convection and radiation (see Fig. 2D and fig. S3 for details). Our simulation also showed that the higher k_p achieved with the addition of the AlN microparticles reduces the peak-to-peak temperature variation on the stretchable sheets by up to 70% (from 2.7° to 0.7°C) and, eventually, reduces the power consumption by up to 40% at 6.6°C of TED cooling effect (fig. S3, B and E). In addition, the simulation results indicate that the thermal conductivity of our Ecoflex/AlN mixture layer (0.77 W m^{-1} K^{-1}) is sufficient to achieve minimal power consumption (or maximal cooling effect) because the temperature variation within the Ecoflex/AlN mixture layer is already sufficiently small (0.7°C) compared to the temperature difference between the hot side and ambient temperature (~10°C) (fig. S3, B and F).

We also demonstrated the flexibility and mechanical robustness of the TED by monitoring the electrical resistance in real time under bending conditions using various bending radii (r). The resistance of the TED was stable when r was reduced to 20 mm (Fig. 2E), which represents the largest curvature of a human body. The resistance of the device was also stable during 1000 bending cycles for r = 30 mm (Fig. 2F). These results demonstrate the excellent flexibility of the TED enabled by our double elastomer layer design embedding rigid TE pillars between two thin, stretchable Ecoflex sheets.

Power generation performance of flexible TED

With the use of the air gap insulation layer and the optimal thermal design of high-ZT TE pillars, our TED surpasses the performance of all previously reported flexible or wearable TEDs, which is the key reason why our device is capable of delivering the long-term active cooling effect. As none of the previous devices achieved active cooling effect without the use of heat sinks, here, we demonstrate power generation

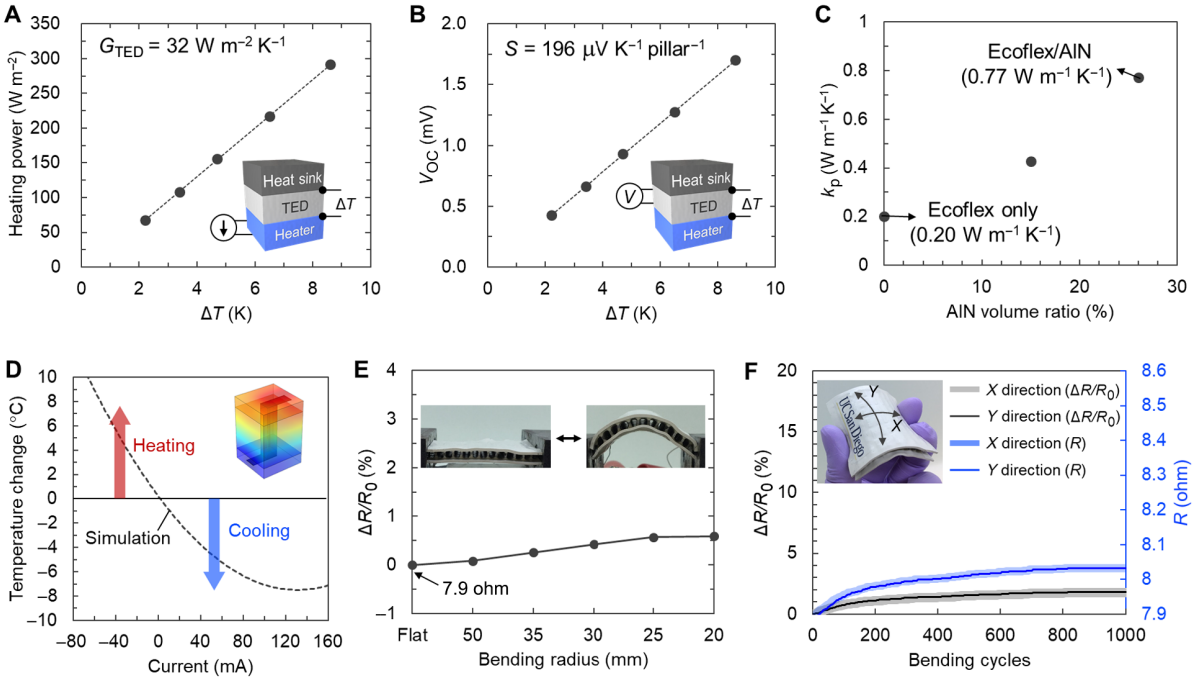

Fig. 2. Characterization of the TED. (**A**) Measurement of the thermal conductance of the TED (G_{TED}). A G_{TED} value of 32 W m^{-2} K^{-1} was determined from the slope of the temperature differences between the cold and hot sides (ΔT) versus the applied heat flux to the underlying heater, when there is no current applied to the TED (i.e., passive mode). (**B**) Measurement of the device-level Seebeck coefficient (S = 196 μV K^{-1}) by comparing ΔT and corresponding open-circuit voltages (V_{OC}). (**C**) Thermal conductivity of the polymeric Ecoflex stretchable sheets (k_p) for various volume ratios of the Ecoflex and AlN microparticles. The mixture layer containing 26 volume % of AlN microparticles exhibited k_p = 0.77 W m^{-1} K^{-1}, which is four times higher than that of pristine Ecoflex (k_p = 0.20 W m^{-1} K^{-1}). (**D**) Finite element simulation of cooling/heating effect with the measured TED parameters. More than 7°C maximum cooling was estimated with only natural convection and radiation. (**E**) Electrical resistance (R) stability for various bending radii (r) from flat to 20 mm, where R_0 is R when the TED is flat, and ΔR is the difference between R and R_0. (**F**) Electrical resistance stability over 1000 bending cycles with r = 30 mm. Photo credit: Sahngki Hong, University of California, San Diego.

from human body heat using our TED and directly compare it to that of previously reported flexible TEDs. During the measurement, our flexible TED was attached to the wearer's arm; the voltage, current, and temperature difference between the cold and hot sides (ΔT) were measured under various load resistances and thermal conditions. A schematic illustration of the measurement setup and the results are presented in Fig. 3 (A to C). When the wearer was sitting stationary in an indoor environment at 22°C, the maximum open-circuit voltage (V_{OC}) was 74.5 mV and the maximum power density of our flexible TED on 32°C human skin was 4.5 μW cm^{-2}. This is the highest generated power density ever reported for wearable TE generators on human skin without heat sinks. Previous wearable TE generators based on a wide variety of materials and designs without heat sinks (*18*–*26*, *33*–*35*) have exhibited maximum power densities of up to 2.28 μW cm^{-2} on human skin (*21*), as summarized in Fig. 3D. Furthermore, the power density increased to 10.7 μW cm^{-2} when the wearer was walking at a speed of 5 km hour^{-1} because of the increase in h_{air} (19.6 W m^{-2} K^{-1}) (*37*) and to 25.1 μW cm^{-2} in a cold indoor environment (10°C). The maximum power generation versus ΔT on the skin followed the same trend as that on the heater setup (Fig. 3C).

The high performance in power generation of our flexible TED originated from the use of high-ZT inorganic TE materials in a flexible form and our optimal thermal design, namely, a low G_{TED} that matches human metabolic heat and natural convection conditions, which are also the two prerequisites to achieve active cooling on human skin without a heat sink, as discussed earlier. To further illustrate this point, we investigated the relationship between the power generation (Seebeck effect) and the cooling effect (Peltier effect) as a function of G_{TED} and ZT through simulation. We set the human metabolic heat (Q_{skin}) to 87 W m^{-2} and h_{air} to 10 W m^{-2} K^{-1} with natural convection and radiation. As shown in Fig. 3E, the power generation and cooling effect followed the same increasing trend with decreasing G_{TED}. When the ZT of the TED was 0.7, the device only provided an appreciable (>3°C) cooling effect when G_{TED} was less than 120 W m^{-2} K^{-1}, which corresponds to a power generation density higher than 4 μW cm^{-2}. The required G_{TED} would be even lower if the device had a lower ZT. Because of the low power generation of most previous flexible TE generators without heat sinks (<2.28 μW cm^{-2}), it was challenging to achieve an appreciable cooling effect on human skin.

Cooling and heating performance of flexible TED on simulated heater

We characterized the cooling and heating effect of the TED using a laboratory setup (Fig. 4A). The thin-film heater in the setup generated a heat flux of 87 W m^{-2} to simulate the typical metabolic rate from a human in an indoor environment (*5*). The cooling and heating performance were evaluated by monitoring the temperature at the bottom of the TED (T_c) while a current (I) ranging from −60 to 140 mA was applied to the TED. The negative and positive currents resulted in heating and cooling effects, respectively, as expected from the TED configuration. At each applied current, T_c began changing instantaneously and reached a plateau within a few minutes (Fig. 4B).

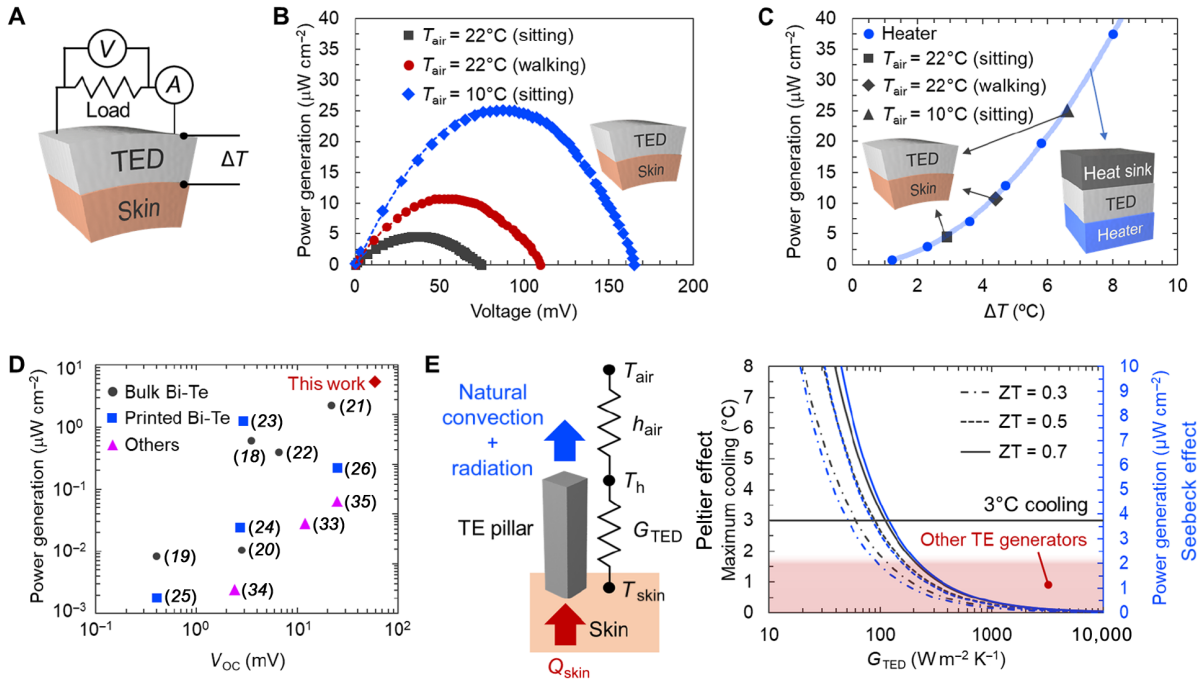

Fig. 3. Power generation of the TED and its impact on active cooling. (**A**) Schematic diagram of the measurement setup used to monitor power generation on human skin. The voltage and current were measured with various load resistors while the TED was attached to the wearer's arm. (**B**) Power generation as a function of output voltage under various thermal conditions. (**C**) Summary of the maximum power generation from our TED on a heater or human skin. The maximum power generation on human skin was 4.5 μW cm^{-2}, and the open-circuit voltage (V_{OC}) was 74.5 mV at room temperature (T_{air} = 22°C) with natural convection (sitting). The power generation increased up to 10.7 μW cm^{-2} with mild forced convection (walking) and up to 25.1 μW cm^{-2} under cold conditions (sitting, T_{air} = 10°C). (**D**) Summary of power generation and V_{OC} of wearable TEDs from the literature. All the measurements were performed on human skin without heat sinks at room temperature. (**E**) Simulation results comparing cooling (Peltier effect, black) and power generation (Seebeck effect, blue) performance as functions of G_{TED} and ZT (right) and schematic illustration of the geometry and thermal conditions used in the simulation (left).

When I = 140 mA, a large steady-state temperature reduction of 7.3°C was achieved with only natural convection and radiation. This cooling effect could be maintained for an extended period (~8 hours) (Fig. 4C).

The stabilized temperature change as a function of the applied current is shown in Fig. 4D. As expected from our finite element model (Fig. 2D), T_c could be deterministically decreased or increased by applying positive or negative current, respectively, due to the Peltier and Joule heating effects. The cooling effect (T_c reduction) was eventually saturated and then diminished with increasing positive current because of the excessive Joule heating. Because of the flexibility of the TED, the cooling and heating effects did not change on a curved substrate with bending radii of 40 and 30 mm (Fig. 4E). We also determined the coefficient of performance (COP) of the devices (right axis in Fig. 4D), which is the ratio between the heat removed from the skin (87 W m^{-2}) and the applied electric power (see Materials and Methods for details). The COP values were measured to be 1.7 and 7.6 for 7°C cooling and heating, respectively. The high COP values indicate a low power consumption of ~90 W for cooling and ~20 W for heating per person assuming total metabolic heat of ~150 W for a human body area of 1.8 m^2.

We also tested the operation of the TED under a mild convection condition with a wind speed of 5 km hour^{-1}. This wind speed can be expected in certain indoor (*38*) and outdoor environments (e.g., walking) (*37*) and will lead to a moderate increase of h_{air}. As shown in Fig. 4F, the maximum cooling was greater than 13°C, approximately twice of that under the natural convection condition because of the more efficient heat dissipation to the air. Using COMSOL modeling, we determined that this temperature reduction corresponds to h_{air} of ~20 W m^{-2} K^{-1} (fig. S3D), which is expected for the 5 km hour^{-1} wind speed.

As previously discussed, the high performance of the TED can be attributed to the unique thermal design: thermal insulation between the cold and hot sides and lateral heat spreading within the Ecoflex/AlN layers. The TE pillars with a small height-to-width ratio in traditional TEDs result in large thermal leakage (large G_{TED}), which diminishes the cooling performance. To verify the thermal design concept, we characterized the cooling/heating performance of a commercial TED (430857-500, Laird Technologies) and three flexible TEDs with various pillar designs for comparison (fig. S5A). A clear trend of enhanced cooling/heating effect was observed with increasing height-to-width ratios of the TE pillars, as shown in fig. S5B. Similar trends were also observed with increasing gap between pillars and increasing lateral thermal conductivity of the elastomer sheets.

We further demonstrated thermoregulation performance of the TED, namely, maintaining a constant skin temperature within a wide range of ambient temperature, with a simulated human skin setup (Fig. 4G). The setup simulated 37°C of constant body core temperature (T_{core}) using a feedback-controlled heater and heat transfer within a 1.2-cm-thick polydimethylsiloxane (PDMS) layer that represented the human skin, which has similar thermal conductance as that of the skin (G_{skin} = 11 to 17 W m^{-2} K^{-1} under comfortable conditions) (*39*). We used a temperature-controlled chamber to encompass the setup and changed the ambient temperature during the demonstration. The TED and a proportional-integral-derivative (PID) controller were programmed to maintain surface temperature of the PDMS layer (T_{skin}) constant, while the ambient temperature was increased from 19° to 33°C

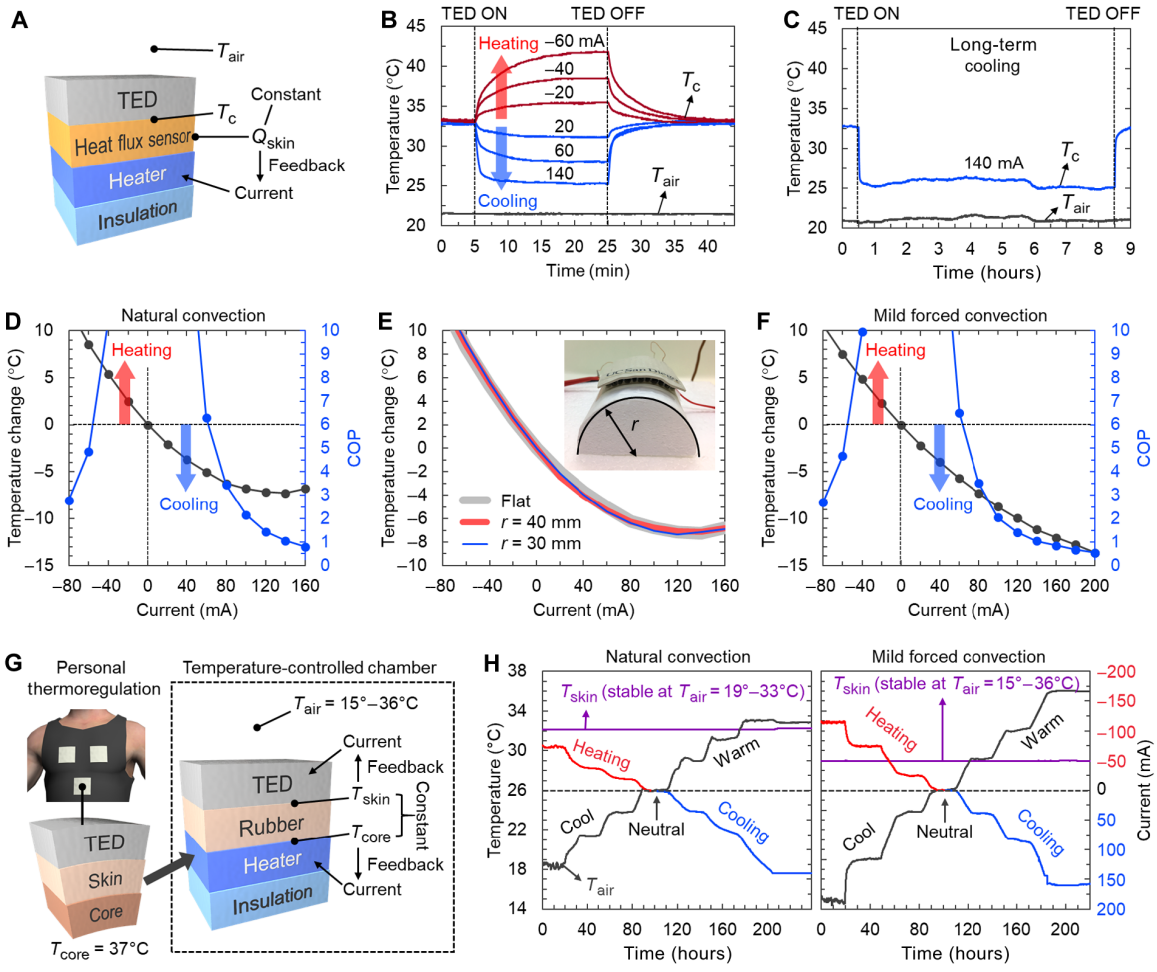

Fig. 4. Cooling and heating performance. (**A**) Laboratory cooling/heating measurement setup. The heating power of a heater (Q_{skin}) was fixed at 87 W m^{-2} (measured by a heat flux sensor) to simulate the typical metabolic rate from a human. (**B**) Time-dependent cooling/heating effects from the TED. (**C**) Sustainable cooling effect for a long period (8 hours) with an electrical current of 140 mA. (**D**) Summary of temperature changes (black) and coefficient of performance (COP) (blue) during TED operation with natural convection. The maximum temperature decrease was 7.3°C. (**E**) Summary of temperature changes (black) and COP (blue) during TED operation with mild forced convection (5 km hour^{-1} wind). The maximum temperature decrease was more than 13.6°C. (**F**) Cooling/heating effects for bending radii (*r*) of 30 and 40 mm, showing no change compared with those on the flat setup. The inset shows the measurement setup to test the cooling/heating effect of the TED under bending. (**G**) Schematic of a human skin setup to demonstrate TED thermoregulation. (**H**) Thermoregulation measurement results. The surface temperature of the polydimethylsiloxane layer (T_{skin}) was maintained by TED cooling and heating within the entire range of ambient temperature. Photo credit: Sahngki Hong, University of California, San Diego.

under the natural convection condition and from 15° to 36°C under the mild forced convection condition (5 km hour^{-1} wind).

As shown in Fig. 4H, within the entire ambient temperature range, the TED could maintain T_{skin} at its set point, the neutral skin temperature at the neutral ambient temperature (26°C), by cooling and heating. The negative or positive currents for TED cooling were applied by the PID controller to compensate the lower or higher ambient temperature, respectively, than the neutral ambient temperature. The results indicate that the TED thermoregulation can provide thermally comfortable condition to a human body within a 14°C temperature span (19° to 33°C) under natural convection condition. With the mild forced convection, this ambient temperature window can even broaden up to 21°C (15° to 36°C). The hottest ambient temperature (33°C) under the natural convection condition was 7°C higher than the neutral ambient temperature, and the TED cooling successfully maintained T_{skin} with 140 mA of applied current. This suggests 7°C cooling effect of the TED, which matches with the maximum temperature drop shown in Fig. 4D. Under the mild forced convection condition, the cooling effect was even larger; the TED could maintain T_{skin} with 160 mA of applied current at the ambient temperature as high as 36°C, which is 10°C higher than the neutral ambient temperature. Considering that the TED showed extra cooling effect when the current was larger than 160 mA (Fig. 4F), the cooling effect of the TED under the mild forced convection condition can be greater than 10°C.

Thermoregulation on human skin using flexible TED

The flexibility of our TED makes it well suited for personalized thermoregulation as a wearable device. To demonstrate personalized thermoregulation on human skin under realistic conditions, we integrated the flexible TED into a garment and attached it onto the arm of a human subject. As shown in Fig. 5A, we used a thin porous mesh fabric to cover the TED without impeding the heat dissipation, while we used an elastic nylon fabric to wrap the TED around the arm. We used a thermocouple to monitor the temperature of the skin covered by the TED (T_{skin}), while

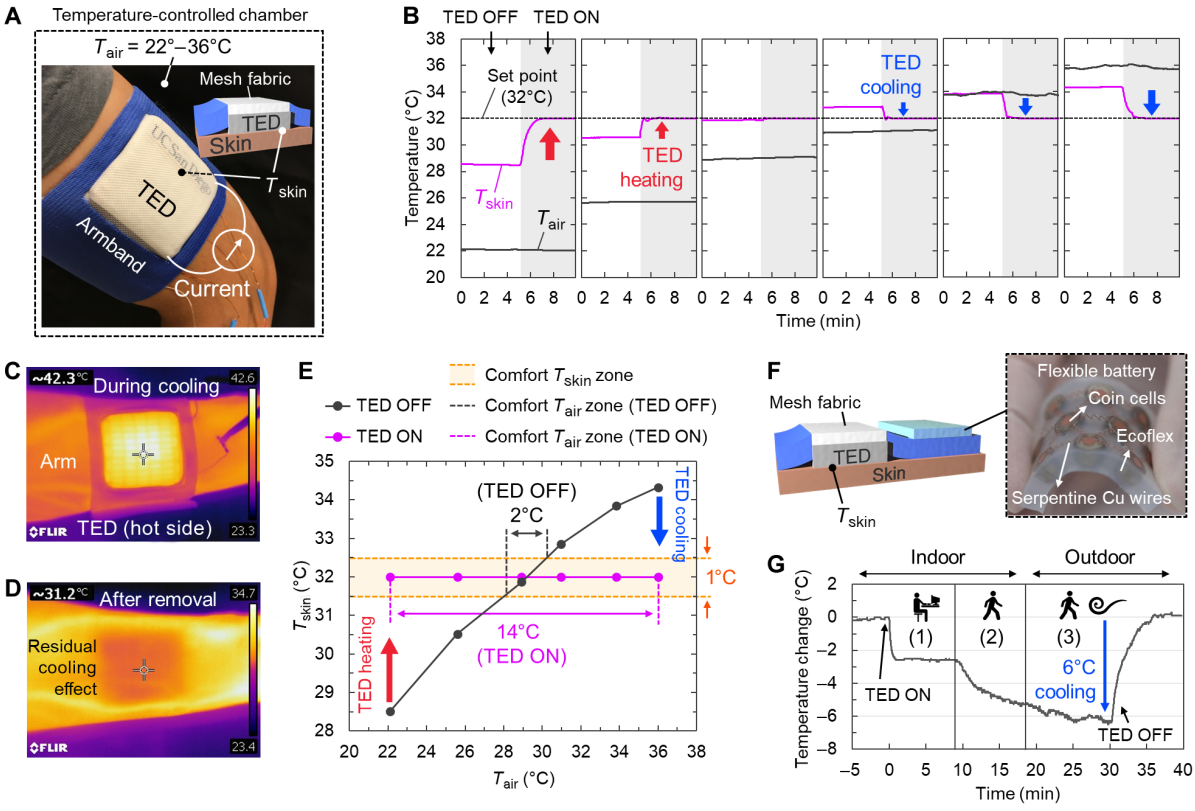

Fig. 5. Demonstration of thermoregulation on human skin. (**A**) Photograph and schematic diagram of the TED armband. The wearer's arm was encompassed by a controlled thermal environment. (**B**) Change in T_{skin} under various T_{air} conditions before and after TED operation. Without TED operation, T_{skin} varied from 28.5° to 34.3°C, while T_{air} changed from 22° to 36°C. With active thermoregulation of the TED, T_{skin} converged to the preset comfort temperature (32°C) under all the T_{air} conditions. (**C**) IR image of the TED armband (hot side) during cooling (I = 160 mA) on the subject's arm. (**D**) IR image of the skin after removing the TED armband, showing residual cooling effect. (**E**) Summary of T_{skin} as a function of T_{air} with and without TED operation. The cooling and heating of the TED broadened the comfortable ambient temperature zone from 2°C (T_{air} = 28° to 30°C) to 14°C (T_{air} = 22° to 36°C). (**F**) Schematic of the TED armband integrated with the flexible battery pack (photograph). (**G**) Skin temperature change by TED cooling under three conditions: (1) sitting indoors, (2) walking indoors, and (3) walking outdoors under mild wind conditions. The maximum skin cooling effect was 6°C. Photo credit: Sahngki Hong, University of California, San Diego.

the subject was exposed to a controlled thermal environment within a wide temperature span of 22° to 36°C. We then used an external PID controller (programmable temperature controller PTC10, Stanford Research Systems) to adjust the current applied to the TED to maintain T_{skin} at the comfort temperature (32°C) regardless of the ambient temperature. At each ambient temperature set point (namely, 22°, 26°, 29°, 31°, 34°, and 36°C), the current to the TED was initially turned off (TED OFF) during the first 5 min, and the corresponding T_{skin} was monitored, as shown in Fig. 5B. As expected, the T_{skin} largely followed the ambient temperature: Tskin varied from 28.5° to 34.3°C as Tair was changed from 22° to 36°C. After the first 5 min, the TED was turned on with its applied current automatically adjusted by the PID controller with a temperature set point of 32°C. As shown in Fig. 5B, the measured skin temperature reached the set point within 2 min and then remained at the set temperature thereafter regardless of whether the ambient temperature was lower (heating from TED) or higher (cooling from TED). This fast thermal response from the TED followed the same behavior as the laboratory setup (Fig. 4B). The precise and adjustable skin temperature control offered by the TED highlights the unique advantages of TE thermoregulation compared with other approaches, such as water or ice packs, which are not controllable.

We also used an IR camera (E60, FLIR) to image the skin and TED to visualize the active heat pumping effect. Figure 5C shows the TED hot-side temperature of approximately 42°C for the maximum cooling condition, which illustrates the active heat pumping from the cold (skin) side to the hot side. The hot-side temperature is also consistent with h_{air} (~11 W m^{-2} K^{-1}) and the heat dissipation to the environment (skin metabolic heat plus TED power consumption; see note S2). Figure 5D presents an IR image of the residual cooling effect on the skin immediately after removing the TED. The IR image shows ~2.5°C cooling on the skin under the area originally covered by the TED compared with the rest of the skin.

The achievement of precisely controllable thermoregulation using the flexible TED has significant implications, which can be best illustrated by the distinctly different skin temperature responses to ambient temperature variation with and without TED operation (Fig. 5E). The typical comfort temperature range of human skin is 31.5° to 32.5°C, which corresponds to an ambient temperature range of 28° to 30°C without the TED (*39*, *40*). When the TED is operating, however, the skin temperature can be maintained at a constant comfort temperature of 32°C even within the wider ambient temperature range of 22° to 36°C, thus simultaneously broadening the comfortable ambient temperature zone from 2°C (T_{air} = 28° to 30°C) to 14°C (T_{air} = 22° to 36°C) and enhancing the wearer's thermal comfort. This 14°C of comfortable ambient temperature zone with the TED operation matches with the results obtained by our PDMS setup that simulated human skin

(Fig. 4H). The broadening of the ambient temperature set points could lead to substantial energy savings for indoor centralized HVAC systems, by as much as ~0.8 kW per person or 20% for a typical building, according to energy analysis (*1*, *10*). Notably, this building-level energy savings is achieved with negligible energy consumption by the TED, as expected from the measured high COP of our TEDs (Fig. 4, D and F). We also directly measured the power consumption of the TED when cooling the skin, which was determined to be only about tens of watts per person, depending on the ambient temperature (see details in fig. S6). Therefore, our results directly point to the tremendous energy-saving potential offered by individualized thermoregulation using our flexible TEDs.

Integration of TED with flexible batteries for mobile thermoregulation

We also demonstrated the mobility of our wearable TED by integrating it with a flexible battery pack to produce an all-flexible personalized thermoregulation device. The power pack was fabricated by embedding 10 coin cell batteries into an Ecoflex matrix and connecting them to each other with serpentine copper electrodes such that their flexibility matched that of the TED (see Materials and Methods for details) (*41*). Figure 5F shows an integrated cooling armband with the flexible battery pack. The device was tested under three realistic conditions to investigate the effect of various convection and metabolic conditions, as shown in Fig. 5G and fig. S7: (1) sitting in an indoor environment without wind to represent typical office conditions, (2) walking indoors at a speed of ~5 km hour^{-1} to test the cooling effect under enhanced metabolic rate and convection conditions, and (3) walking outdoors at a speed of ~5 km hour^{-1} under mild wind conditions to verify the feasibility of the TED for outdoor usage (see Materials and Methods for details).

When the TED was initially turned on with the flexible battery pack (I = 120 mA), the skin temperature decreased rapidly by up to 2.5°C, which matches well with the temperature drop shown in Fig. 5 (B and E). This temperature drop was stable as long as the wearer was sitting still (condition 1). When the wearer started walking under the second condition, the temperature drop doubled, up to ~5°C, because of the forced convection effect during walking, which is consistent with the trend observed in the laboratory setup under the mild forced convection condition (Fig. 4F). The last condition additionally increased the temperature drop to up to 6°C because of the even higher convection effect from the synergy of walking and the wind outside. This 6°C skin cooling effect of the 5 cm by 5 cm TED consumed only ~180 mW of power or 1.8 Wh (watt-hour) of energy for 10-hour operation, which can be supplied by ~9 g of batteries (assuming a battery energy density of ~200 Wh kg^{-1}) (*42*). Considering a cooling vest made of 144 of these TEDs to cover the hot spots on the skin (e.g., back, chest, and abdomen) with an area of ~3600 cm^2 (~20% of the total body area), the power consumption is calculated to be ~26 W. Moreover, under the mild forced convection, the power consumption of the cooling vest is expected to be reduced by ~45%, to ~14.3 W, based on the results from the laboratory setup (Fig. 4F). This energy consumption can be readily supplied by a battery pack with a weight of ~430 g for approximately 6 hours of operation.

In summary, we have developed a flexible and wearable TED with large, sustainable, controllable cooling and heating effect with a high COP for personalized thermoregulation. The TED is sufficiently thin, flexible, light, and readily embeddable into a garment. The wearability of the TED is uniquely achieved by eliminating the need for the large heat sinks (e.g., fin or fan) typically used in traditional devices and by exploiting high-aspect-ratio TE pillars embedded with double elastomer layers with air gap thermal insulation to achieve low thermal conductance in the TED and high flexibility. We achieved a large cooling effect of more than 10°C in the TED without the use of a heat sink, which will provide sufficient thermoregulation for human thermal comfort. We also integrated the TEDs into a wearable garment and demonstrated the long-term, energy-efficient cooling and heating effects on human skin: The garment maintained skin at the comfort temperature of 32°C while the ambient temperature varied from 22° to 36°C. The high COP of the TED and the localized cooling capability offer tremendous energy-saving potential for personalized cooling compared with traditional centralized space cooling approaches. Thus, wearable garments based on the TED developed in this work may revolutionize cooling technology for climate control in buildings and vehicles.

MATERIALS AND METHODS

Fabrication of flexible TED

The processes used to fabricate the flexible TED are schematically illustrated in Fig. 1F. First, commercial TE alloys were cut into pillars that were 1 mm by 1 mm in area and 5 mm in height [TEC1-07101, Thermonamic Electronics (Jiangxi) Corp. Ltd.]. The TE pillars were aligned into a 12 × 12 array with 3-mm spacing between adjacent pillars. The array was attached to a carrier substrate using a thermal-responsive adhesive as the first step. A Cu film (35 μm in thickness) with a solvent-soluble adhesive (76555A725, McMaster-Carr) was attached to another carrier substrate for the fabrication of the top electrodes. The Cu film on the carrier substrate was cut into individual electrodes (1.5 mm in width and 5.5 mm in length) for each pair of TE pillars, and the residual Cu film was removed from the carrier substrate (fig. S1A). A polyimide (PI) tape was attached to the electrodes as a solder mask opening only the parts that contact with the TE pillars. The Cu electrodes on the carrier substrate were soldered to the TE pillar array using a soldering paste (SMDLTLFP50T3, Digi-Key) (fig. S1C). After detaching the carrier substrate and solder mask from the Cu electrodes by soaking the device in acetone, a SiO_2 layer (200 nm) was deposited onto the electrodes to improve the adhesion with the stretchable polymer sheet. Next, 1-mm-thick Ecoflex 00-30A/B (Smooth-On) containing 26 volume % of AlN powder (10 μm in diameter; Sigma-Aldrich) was cured, embedding the electrodes and the small segment (0.5 mm) of TE pillars. The Ecoflex and AlN powder mixture film with the electrodes and TE pillars was cut to dimensions of 5 cm by 5 cm, and the carrier substrate for the TE pillars was detached by applying heat to melt the heat-responsive adhesive. The aforementioned process was repeated for the bottom layer fabrication.

TE characterization of TED

The thermal conductance of the TED (G_{TED}) was measured by applying heating power (Q) to the TED and measuring the temperature difference between the hot and cold sides ($\Delta T = T_h - T_c$, where T_h is the hot side temperature and T_c is the cold side temperature). G_{TED} was calculated using $G_{TED} = d(Q)/d(\Delta T)$. The Seebeck coefficient (S) was also measured using the same setup by additionally measuring V_{OC} of the TED for various temperature differences. The device-level average Seebeck coefficient was calculated from the slope of V_{OC} versus ΔT, namely, $S = d(V_{OC})/d(\Delta T)$. The thermal conductivity of the stretchable Ecoflex sheets (k_p) was measured using the same method as that used for the G_{TED} measurement, and the measurement was

calibrated with standard polymer samples, including pristine Ecoflex (k_p = 0.20 W m^{-1} K^{-1}).

Measurement of cooling/heating performance of TED

For the laboratory setup shown in Fig. 4A, a thin-film heater and a heat flux sensor (PHFS-01, FluxTeq) were used to simulate metabolic heat from a human body. During the measurement, the heater power was PID controlled to maintain a constant heat flux (fig. S4). A polystyrene foam insulation layer was placed underneath the heater to prevent parasitic heat loss. A thermocouple was placed under the TED to measure T_c, and the other thermocouple was located ~20 cm away from the TED to monitor the ambient temperature (T_{air}). The cooling and heating effect at each electrical current was measured for 60 min: 20 min for prestabilization of the temperature without an electrical current, 20 min of TED operation with the current ranging from −80 to 160 mA (−80 to 200 mA for the forced convection condition), and 20 min of poststabilization of temperature after switching off the electrical current. The temperature change in the summary results (e.g., Fig. 4D) was defined by the temperature difference of T_c shortly before switching on and off the TED. The cooling/heating measurements were repeated three times (fig. S3, C and D), and the root mean square error was less than 0.3°C. The temperature increased when a negative current was applied to the TED and decreased when a positive current was applied. For cooling, with increasing current, the temperature decreased almost linearly because of the Peltier effect and then began to saturate and eventually increased because of the excessive Joule heating. However, when a negative current was applied for heating, the temperature continued rising without saturation as the electrical current decreased because of the combined Peltier and Joule heating effects.

The COP was determined using

$$\mathrm{COP} = \frac{Q_{skin}}{W} = \frac{Q_{skin}}{SI\Delta T + I^2R} \quad (1)$$

where Q_{skin} is the metabolic heat from a human body (Q_{skin} = 87 $W\ m^{-2} \times A$), A is the area of the TED, W is the supplied power, I is the applied electrical current, and R is the internal electrical resistance of the TED.

Measurement of TED performance on human subject

The armband was fabricated by attaching a piece of mesh fabric (90% nylon and 10% spandex) onto a square hole (~6 mm by 6 cm) of a nylon elastic fabric strip with fabric adhesive. The TED was sandwiched between the mesh fabric and skin during the measurement. A healthy male subject with normal body mass index was recruited, and the cooling/heating effect of the TED armband was measured on the wearer's arm, as shown in Fig. 5A. TED performance tests on the human subject were conducted in strict compliance following a protocol approved by the Institutional Review Board at University of California, San Diego (project no. 130003). A temperature-controlled chamber was designed to locally regulate the ambient temperature (T_{air}) near the arm considering the small areal density of the TED relative to the surface of a human body. T_{air} in the chamber was controlled by a heater with thermally insulating fabric covering the chamber to prevent heat loss. A small hole in the chamber was prepared to place the subject's arm. Before the measurement, the subject sat and relaxed under a thermal comfort condition while placing an arm in the chamber and waited for more than 1 hour for stabilization of the metabolic condition and T_{air} in the chamber. There were no sources of forced airflow such as movement of the subject or ventilation during the measurement. The current applied to the TED was PID controlled to maintain T_{skin} at the comfort temperature of 32°C (Fig. 5B). After T_{skin} reached steady state, T_{skin} and T_{air} were recorded for 10 min, and the TED was switched after 5 min.

Fabrication of flexible battery pack

A piece of copper sheet (a thickness of 20 μm; Oak-Mitsui Inc.) was first spin-coated with the amic acid precursor [poly(pyromellitic dianhydride-co-4,40-oxydianiline); HD-PI2545, HD MicroSystems], followed by soft baking at 110°C for 3 min and at 150°C for 1 min to fully remove the solvents. The thickness of the PI film after baking was 2 μm, which was determined from the spin-coating parameters (4000 rpm, 1 min). Hard baking of the PI film was performed at 300°C for 1 hour in a nitrogen gas oven to achieve complete cross-linking and curing of the PI. The copper/PI sheet was then laminated on a piece of glass slide coated with PDMS (SYLGARD 184 silicone elastomer; 15:1) with the PI layer contacting the PDMS. Before lamination, both the PI and PDMS surfaces were activated with ultraviolet (UV) light (PSD series Digital UV Ozone System, Novascan) for 2 min. The island-bridge serpentine structure was designed with AutoCAD software and then patterned using pulsed laser ablation (Laser Mark's) on the copper sheets. The laser parameters (central wavelength of 1059 to 1065 nm, power of 0.228 mJ, frequency of 35 kHz, speed of 300 mm s^{-1}, and pulse width of 500 ns) were optimized for the copper sheet ablation. In a coin cell battery array, two such electrodes, a cathode (+) and an anode (−), are needed. The patterned electrode was then transfer-printed with a water-soluble tape (3M) to a silicone superstrate/substrate (300 μm; Ecoflex, Smooth-On Inc.) with the PI layer contacting the silicone layer. The Ecoflex superstrate was prepared by mixing two parts of its precursor components (1:1 volume ratio), spin coating at 100 rpm for 1 min, and cross-linking on a hot plate at 60°C for 30 min. To improve the bonding strength between PI and the Ecoflex layer, UV activation was applied followed by baking at 80°C for 10 min in a convection oven. The water-soluble tape was rinsed off with deionized water.

For these tests, we adopted coin cell batteries operated by an aqueous-based electrolyte (XR48, ZPower LLC.). These batteries provide a stable and nonflammable electrochemistry, which is suitable for wearable applications. The coin cells were connected in parallel and bonded to the first copper electrode with a silver-epoxy conductive adhesive (EPO-TEK H20E, Epoxy Technology) at 80°C for 4 hours in a convection oven. The second electrode was aligned with the prebonded coin cells under a stereomicroscope and bonded with the silver-epoxy adhesive using the same method. Next, two copper wires were soldered to the specific island pads on both the anodic and cathodic copper electrodes. Then, the gap between the sandwiched device was filled with Ecoflex and cured at room temperature for 4 hours. Last, a free-standing stretchable coin cell battery array was obtained after removing the two pieces of glass slides.

Demonstration of mobile application of TED with flexible battery pack

Two identical TED armbands were prepared for this demonstration. The TED armbands were attached to both of the subject's arms; one of the TEDs was operated using the flexible battery pack during the demonstration, while the other was not operated (fig. S7A). Along with the skin temperature under the TED with operation (T_{skin}), the skin

temperature under the TED without operation ($T_{skin,ref}$) was monitored as a reference to compensate for the passive cooling/heating effects by thermal condition changes (e.g., wind, ambient temperature, or metabolic heat generation). The relative temperature change (ΔT_{rel}) from the active TED cooling was calculated using $T_{rel} = (T_{skin,\ ref} - T_{skin}) - (T_{skin,\ ref} - T_{skin})_{t\ =\ 0}$. The similar T_{skin} and $T_{skin,ref}$ values before and after measurement (fig. S7B) indicate that both arms and TEDs were exposed to identical thermal conditions (e.g., thermal insulation and metabolic heat generation).

SUPPLEMENTARY MATERIALS

Supplementary material for this article is available at http://advances.sciencemag.org/cgi/content/full/5/5/eaaw0536/DC1

Note S1. Theoretical analysis of thermal design parameters to achieve active cooling of TED on human skin

Note S2. Theoretical verification of the hot side temperature and heat flux during TED cooling on human skin

Fig. S1. Fabrication and characterization of the TED.

Fig. S2. Optimization of the TED.

Fig. S3. COMSOL modeling of the TED cooling effect.

Fig. S4. PID control of the heat flux from the heater.

Fig. S5. Comparison of TEDs.

Fig. S6. Measurement system and power consumption of the thermoregulation on human skin.

Fig. S7. Temperature change during the mobile thermoregulation demonstration.

REFERENCES AND NOTES

1. J. D. Kelso, *2011 Buildings Energy Data Book* (U.S. Department of Energy, 2012).
2. S. Chu, A. Majumdar, Opportunities and challenges for a sustainable energy future. *Nature* **488**, 294–303 (2012).
3. R. Farrington, J. Rugh, *Impact of Vehicle Air-Conditioning on Fuel Economy, Tailpipe Emissions, and Electric Vehicle Range* (NREL/CP-540–28960, 2000); www.nrel.gov/docs/fy00osti/28960.pdf.
4. E. A. Goldstein, A. P. Raman, S. H. Fan, Sub-ambient non-evaporative fluid cooling with the sky. *Nat. Energy* **2**, 17143 (2017).
5. W. L. Kenney, J. Wilmore, D. Costill, *Physiology of Sport and Exercise* (Human Kinetics, ed. 6, 2015).
6. R. J. de Dear, G. S. Brager, Developing an adaptive model of thermal comfort and preference. *ASHRAE Trans.* **104**, 145–167 (1998).
7. M. Mokhtari Yazdi, M. Sheikhzadeh, Personal cooling garments: A review. *J. Text. Inst.* **105**, 1231–1250 (2014).
8. P.-C. Hsu, C. Liu, A. Y. Song, Z. Zhang, Y. Peng, J. Xie, K. Liu, C.-L. Wu, P. B. Catrysse, L. Cai, S. Zhai, A. Majumdar, S. H. Fan, Y. Cui, A dual-mode textile for human body radiative heating and cooling. *Sci. Adv.* **3**, e1700895 (2017).
9. P.-C. Hsu, X. Liu, C. Liu, X. Xie, H. R. Lee, A. J. Welch, T. Zhao, Y. Cui, Personal thermal management by metallic nanowire-coated textile. *Nano Lett.* **15**, 365–371 (2014).
10. M. Veselý, W. Zeiler, Personalized conditioning and its impact on thermal comfort and energy performance–A review. *Renew. Sustain. Energy Rev.* **34**, 401–408 (2014).
11. S.-G. Lu, Q. Zhang, Electrocaloric materials for solid-state refrigeration. *Adv. Mater.* **21**, 1983–1987 (2009).
12. X. Moya, S. Kar-Narayan, N. D. Mathur, Caloric materials near ferroic phase transitions. *Nat. Mater.* **13**, 439–450 (2014).
13. J. He, T. M. Tritt, Advances in thermoelectric materials research: Looking back and moving forward. *Science* **357**, eaak9997 (2017).
14. R. Ma, Z. Zhang, K. Tong, D. Huber, R. Kornbluh, Y. S. Ju, Q. Pei, Highly efficient electrocaloric cooling with electrostatic actuation. *Science* **357**, 1130–1134 (2017).
15. J.-H. Bahk, H. Fang, K. Yazawa, A. Shakouri, Flexible thermoelectric materials and device optimization for wearable energy harvesting. *J. Mater. Chem. C* **3**, 10362–10374 (2015).
16. F. Suarez, A. Nozariasbmarz, D. Vashaee, M. C. Öztürk, Designing thermoelectric generators for self-powered wearable electronics. *Energ. Environ. Sci.* **9**, 2099–2113 (2016).
17. S. J. Kim, H. E. Lee, H. Choi, Y. Kim, J. H. We, J. S. Shin, K. J. Lee, B. J. Cho, High-performance flexible thermoelectric power generator using laser multiscanning lift-off process. *ACS Nano* **10**, 10851–10857 (2016).
18. F. Suarez, D. P. Parekh, C. Ladd, D. Vashaee, M. D. Dickey, M. C. Öztürk, Flexible thermoelectric generator using bulk legs and liquid metal interconnects for wearable electronics. *Appl. Energy* **202**, 736–745 (2017).
19. S. H. Jeong, F. J. Cruz, S. Chen, L. Gravier, J. Liu, Z. Wu, K. Hjort, S.-L. Zhang, Z.-B. Zhang, Stretchable thermoelectric generators metallized with liquid alloy. *ACS Appl. Mater. Interfaces* **9**, 15791–15797 (2017).
20. H. Liu, Y. Wang, D. Mei, Y. Shi, Z. Chen, Design of a wearable thermoelectric generator for harvesting human body energy. *Wear. Sens. Robots* **399**, 55–66 (2016).
21. C. S. Kim, G. S. Lee, H. Choi, Y. J. Kim, H. M. Yang, S. H. Lim, S.-G. Lee, B. J. Cho, Structural design of a flexible thermoelectric power generator for wearable applications. *Appl. Energy* **214**, 131–138 (2018).
22. Y. Wang, Y. Shi, D. Mei, Z. Chen, Wearable thermoelectric generator to harvest body heat for powering a miniaturized accelerometer. *Appl. Energy* **215**, 690–698 (2018).
23. S. J. Kim, J. H. We, B. J. Cho, A wearable thermoelectric generator fabricated on a glass fabric. *Energ. Environ. Sci.* **7**, 1959–1965 (2014).
24. M.-K. Kim, M.-S. Kim, S. Lee, C. Kim, Y.-J. Kim, Wearable thermoelectric generator for harvesting human body heat energy. *Smart Mater. Struct.* **23**, 105002 (2014).
25. Z. Lu, H. Zhang, C. Mao, C. M. Li, Silk fabric-based wearable thermoelectric generator for energy harvesting from the human body. *Appl. Energy* **164**, 57–63 (2016).
26. S. E. Jo, M. K. Kim, M. S. Kim, Y.-J. Kim, Flexible thermoelectric generator for human body heat energy harvesting. *Electron. Lett.* **48**, 1015–1017 (2012).
27. Y. Eom, D. Wijethunge, H. Park, S. H. Park, W. Kim, Flexible thermoelectric power generation system based on rigid inorganic bulk materials. *Appl. Energy* **206**, 649–656 (2017).
28. C. S. Kim, H. M. Yang, J. Lee, G. S. Lee, H. Choi, Y. J. Kim, S. H. Lim, S. H. Cho, B. J. Cho, Self-powered wearable electrocardiography using a wearable thermoelectric power generator. *ACS Energy Lett.* **3**, 501–507 (2018).
29. H. Park, D. Kim, Y. Eom, D. Wijethunge, J. Hwang, H. Kim, W. Kim, Mat-like flexible thermoelectric system based on rigid inorganic bulk materials. *J. Phys. D Appl. Phys.* **50**, 494006 (2017).
30. H. Park, D. Lee, D. Kim, H. Cho, Y. Eom, J. Hwang, H. Kim, J. Kim, S. Han, W. Kim, High power output from body heat harvesting based on flexible thermoelectric system with low thermal contact resistance. *J. Phys. D Appl. Phys.* **51**, 365501 (2018).
31. S. Shin, R. Kumar, J. W. Roh, D.-S. Ko, H.-S. Kim, S. I. Kim, L. Yin, S. M. Schlossberg, S. Cui, J.-M. You, S. Kwon, J. Zheng, J. Wang, R. Chen, High-performance screen-printed thermoelectric films on fabrics. *Sci. Rep.* **7**, 7317 (2017).
32. K. Nan, S. D. Kang, K. Li, K. J. Yu, F. Zhu, J. Wang, A. C. Dunn, C. Zhou, Z. Xie, M. T. Agne, H. Wang, H. Luan, Y. Zhang, Y. Huang, G. J. Snyder, J. A. Rogers, Compliant and stretchable thermoelectric coils for energy harvesting in miniature flexible devices. *Sci. Adv.* **4**, eaau5849 (2018).
33. J. H. We, S. J. Kim, B. J. Cho, Hybrid composite of screen-printed inorganic thermoelectric film and organic conducting polymer for flexible thermoelectric power generator. *Energy* **73**, 506–512 (2014).
34. J. Y. Oh, J. H. Lee, S. W. Han, S. S. Chae, E. J. Bae, Y. H. Kang, W. J. Choi, S. Y. Cho, J.-O. Lee, H. K. Baik, T. I. Lee, Chemically exfoliated transition metal dichalcogenide nanosheet-based wearable thermoelectric generators. *Energ. Environ. Sci.* **9**, 1696–1705 (2016).
35. Q. Wu, J. Hu, A novel design for a wearable thermoelectric generator based on 3D fabric structure. *Smart Mater. Struct.* **26**, 045037 (2017).
36. G.-H. Kim, L. Shao, K. Zhang, K. P. Pipe, Engineered doping of organic semiconductors for enhanced thermoelectric efficiency. *Nat. Mater.* **12**, 719–723 (2013).
37. R. J. de Dear, E. Arens, Z. Hui, M. Oguro, Convective and radiative heat transfer coefficients for individual human body segments. *Int. J. Biometeorol.* **40**, 141–156 (1997).
38. P. E. J. Baldwin, A. D. Maynard, A survey of wind speeds in indoor workplaces. *Ann. Occup. Hyg.* **42**, 303–313 (1998).
39. A. P. Gagge, J. A. J. Stolwijk, J. D. Hardy, Comfort and thermal sensations and associated physiological responses at various ambient temperatures. *Environ. Res.* **1**, 1–20 (1967).
40. Y. Yao, Z. Lian, W. Liu, Q. Shen, Experimental study on skin temperature and thermal comfort of the human body in a recumbent posture under uniform thermal environments. *Indoor Built Environ.* **16**, 505–518 (2007).
41. A. J. Bandodkar, J.-M. You, N. Kim, Y. Gu, R. Kumar, A. M. Mohan, J. F. Kurniawan, S. Imani, T. Nakagawa, B. Parish, M. Parthasarathy, P. P. Mercier, S. Xu, J. Wang, Soft, stretchable, high power density electronic skin-based biofuel cells for scavenging energy from human sweat. *Energ. Environ. Sci.* **10**, 1581–1589 (2017).
42. R. Van Noorden, The rechargeable revolution: A better battery. *Nature* **507**, 26–28 (2014).

Acknowledgments: We thank Q. Wang for help in measuring thermal conductivity of elastomer sheets and J. Kim for help in setting measurement systems. **Funding:** This work is supported by the Advanced Research Project Agency—Energy (ARPA-E; grant no. DE-AR0000535) under the DELTA (Delivering Efficient Local Thermal Amenities) program. The human subject test portion of the work was funded by a UCSD startup fund allocated to R.C. This work was performed in part at the San Diego Nanotechnology Infrastructure (SDNI) of UCSD, a member of the National Nanotechnology Coordinated Infrastructure, which is supported by the National Science Foundation (Grant ECCS-1542148). **Author contributions:** S.H. designed and fabricated TEDs, performed the experiments and modeling, analyzed the data. Y.G. fabricated and tested the flexible battery pack. J.K.S. prepared and tested

the coin cells. S.H. and R.C. wrote the manuscript. All the authors edited and commented on the manuscript. P.L., J.W., Y.S.M., S.X., and R.C. supervised the research. **Competing interests:** R.C. and S.H. are inventors on a provisional patent related to this work filed by the Regents of the University of California (no. 62/588,175, filed 16 November 2018). The authors declare that they have no other competing interests. **Data and materials availability:** All data needed to evaluate the conclusions in the paper are present in the paper and/or the Supplementary Materials. Additional data related to this paper may be requested from the authors.

Submitted 23 November 2018
Accepted 2 April 2019
Published 17 May 2019
10.1126/sciadv.aaw0536

Citation: S. Hong, Y. Gu, J. K. Seo, J. Wang, P. Liu, Y. S. Meng, S. Xu, R. Chen, Wearable thermoelectrics for personalized thermoregulation. *Sci. Adv.* **5**, eaaw0536 (2019).